Journal for Geophysical Research – Solid Earth

Supporting Information for

Imaging the Mudurnu Segment of the North Anatolian Fault Zone from Waveforms of Small Earthquakes

Bita Najdahmadi [1], Pavla Hrubcová [2*], Václav Vavryčuk [2], and Marco Bohnhoff [1, 3]

[1] Helmholtz-Centre Potsdam, GFZ German Centre for Geosciences, Section 4.2: Geomechanics and Rheology, Potsdam, Germany
[2] Institute of Geophysics, the Czech Academy of Sciences, Prague, Czech Republic
[3] Free University Berlin, Institute of Geological Sciences, Berlin, Germany

Contents of this file

Introduction

This supporting information provides additional information about data and their processing, as well as about for numerical modelling for different filters and different focal mechanisms.

a)

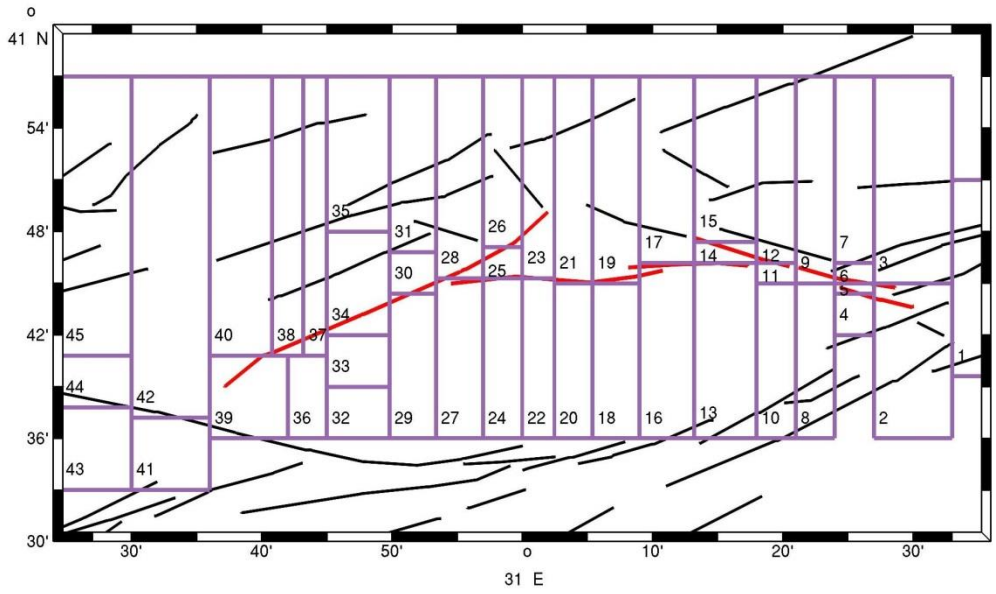

b)

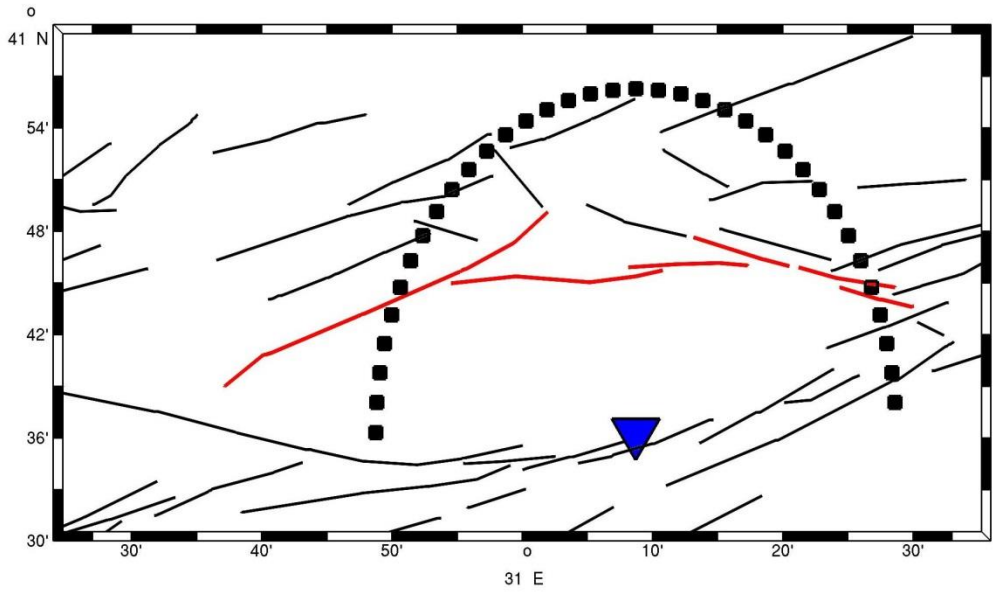

Figure S1. (a) Cluster distribution for depth-sorted seismicity. The seismicity is divided into 45 spatially distributed clusters with similar epicenters (a typical diameter is ~6 km) covering the seismicity on both sides of the Karadere-Düzce fault. In each cluster, the waveforms are sorted according to their depths. Numbering of cluster corresponds to Table S1. (b) Cluster distribution for epicentral-distance sorted seismicity. The seismicity is separated into 36 azimuthally variable segments (numbered from east to west); in each segment, the waveforms are sorted according to the increased epicentral distance.

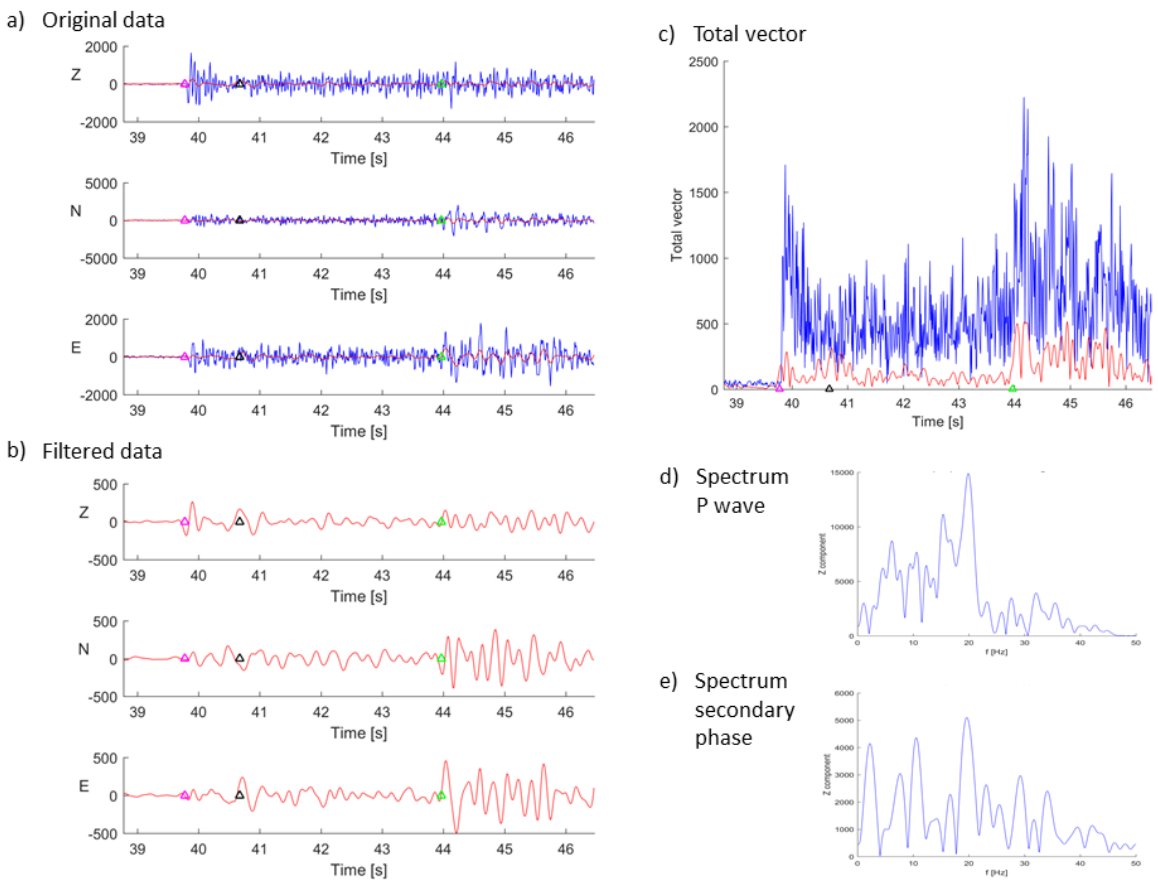

Figure S2. Example of the original and filtered data recorded at station GOK. (a) Non-filtered three-component data for the event e0048.286 from cluster 32 in the north (blue curve). (b) The same data filtered by the Butterworth filter of 1-5 Hz (red curve). (c) Total vector of the same data. The P-wave arrival marked by the red triangle, the S-wave arrival marked by the green triangle, the secondary phase marked by the black triangle. Note the high amplitude of the P wave and the rather small amplitude of the secondary phase in unfiltered data compared to similar amplitudes of the P wave and the secondary phase in the filtered data. (d) Amplitude spectrum of the P wave; (e) amplitude spectrum of the secondary wave. Note the low frequency content of the secondary phase compared to the prevailing frequency of 20 Hz for the direct P wave, explaining the behavior of amplitudes of the P wave and the secondary phase after filtering.

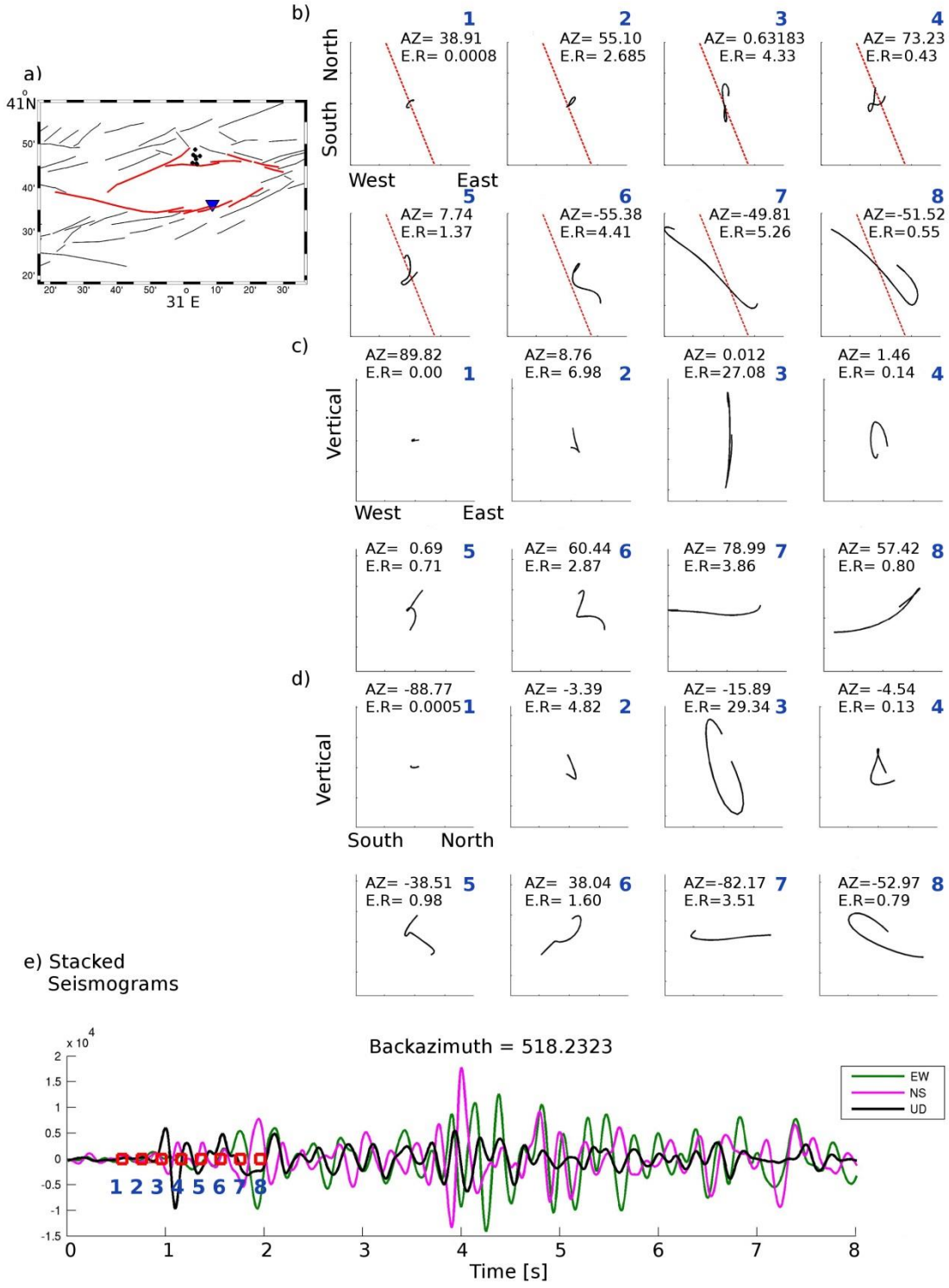

Figure S3. Example of particle motion analysis at station GOK for cluster 21 in the north. (a) Station GOK (blue triangle) and seismicity (black circles) with Karadere, Düzce and Mudurnu faults colored in red. (b) Two-dimensional stacked particle motion of events shown in a) on the

EW-NS planes with a moving time windows (1-8). Each particle motion plot corresponds to a time window marked with a square on the waveforms in e). The dashed red line shows the event-station back azimuth. Azimuth of the largest eigenvalue (AZ) and the ratio of eigenvalues (E.R) are shown in each window as a quantitative tool to track the changes of direction and amplitude of polarization starting from noise in (b-1), direct P arrival in (b-3), minor phase in (b-5) and major phase in (b-7) and (b-8). The values are calculated with the algorithm of *Jurkevics* (1988) and after *Allam and Ben-Zion* (2014). Note the direction of the direct P in (b-3) similar to event-station back azimuth and its change in (b-5) from event-station back azimuth to Mudurnu fault and the polarization of the major phase in (b-7) in accordance with the shear-wave splitting due to anisotropy in the area. (c) Stacked particle motion on the EW-Vertical plane. Particle motion of the direct P wave is vertical in (c-3). The minor phase is weak and rather vertical in (c-5). The major phase is horizontal in (c-7). (d) Stacked particle motion on the NS-Vertical plane. Note the horizontal polarization of the major phase in d-7. (e) Stacked waveforms recorded from the events shown in a) for the EW component seismograms (green), NS components (pink) and vertical components (black). The eight red boxes on the seismograms (numbered in blue) mark centers of the eight windows for which the polarizations are plotted in b), c) and d).

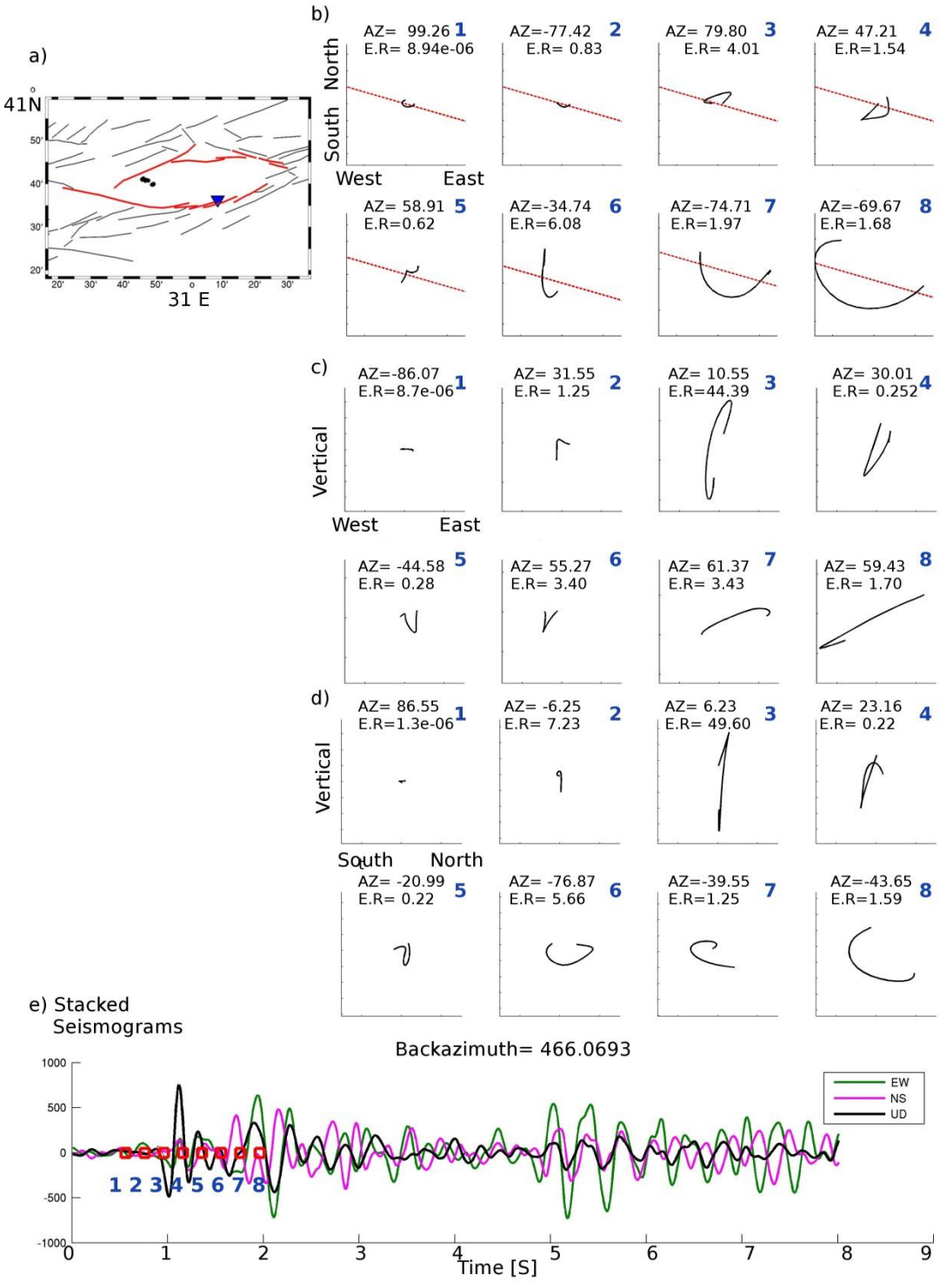

Figure S4. Example of particle motion analysis at station GOK for cluster 33 in the west. The description as in Figure S3.

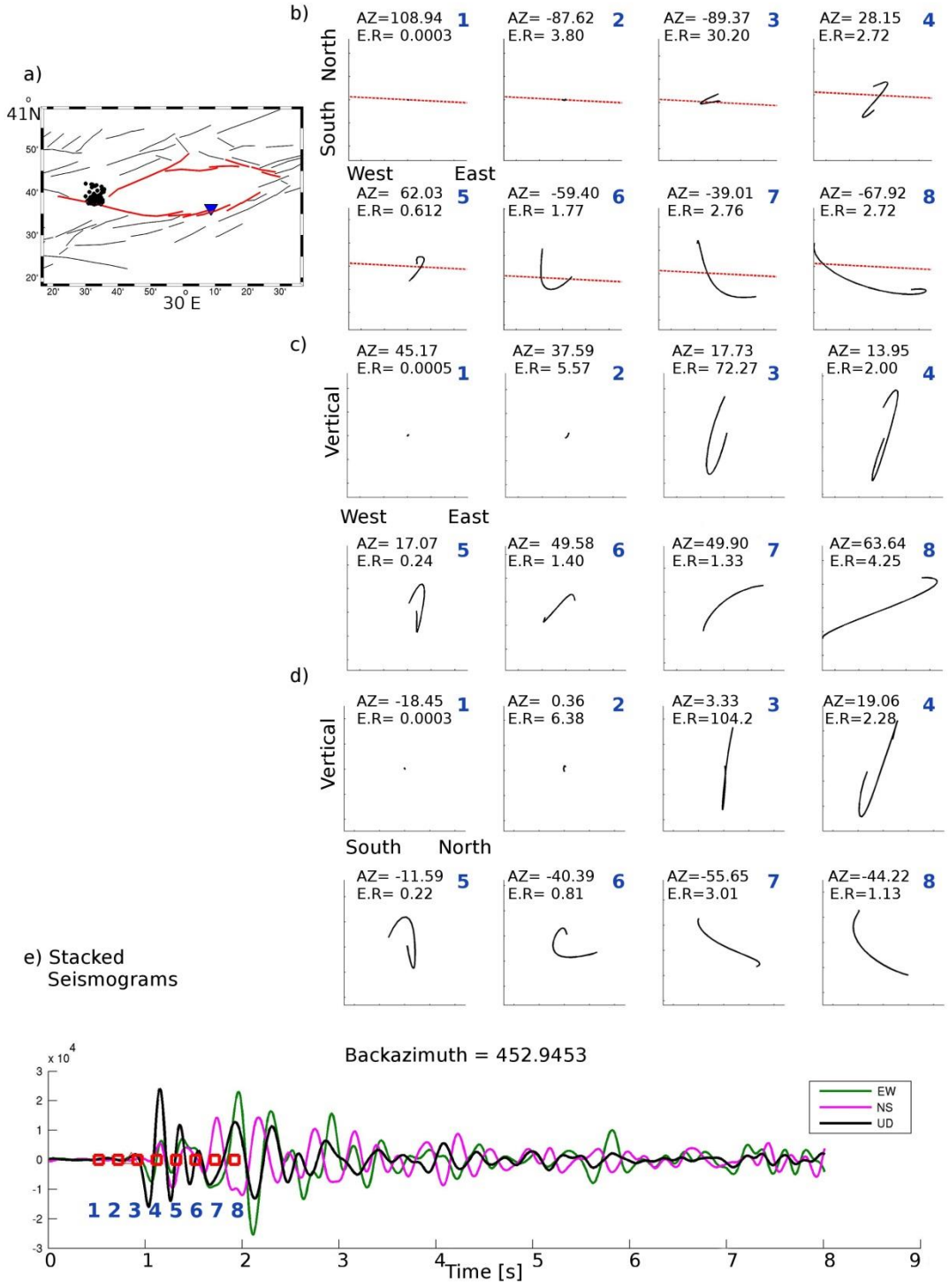

Figure S5. Example of particle motion analysis at station GOK for cluster 42 in the west. The description as in Figure S3.

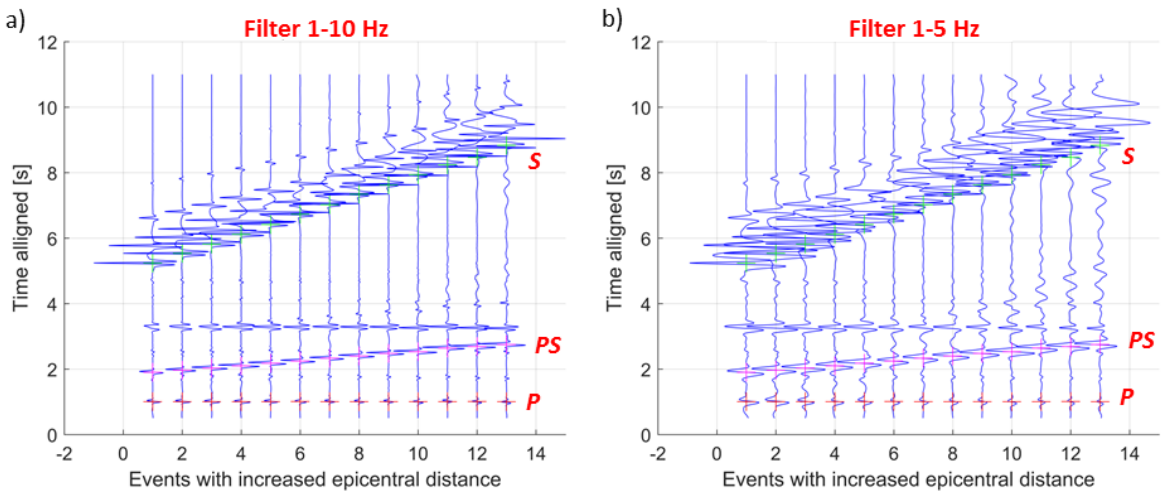

Figure S6. The comparison of synthetic waveforms filtered with Butterworth filter of (a) 1-10 Hz and (b) 1-5 Hz. Vertical component synthetic section for the epicentral-distance-sorted seismicity (epicentral distances range between 30-60 km) at station GOK for a model with a horizontal interface with reverse velocity contrast (downward velocity decrease from 6 to 5 km s^{-1}) at a depth of 3 km. Geometry and focal mechanism as in Figure 11b. Note the sharper onsets of phases for filtering of 1-10 Hz compared to much blurred onsets of phases for filtering of 1-5 Hz.

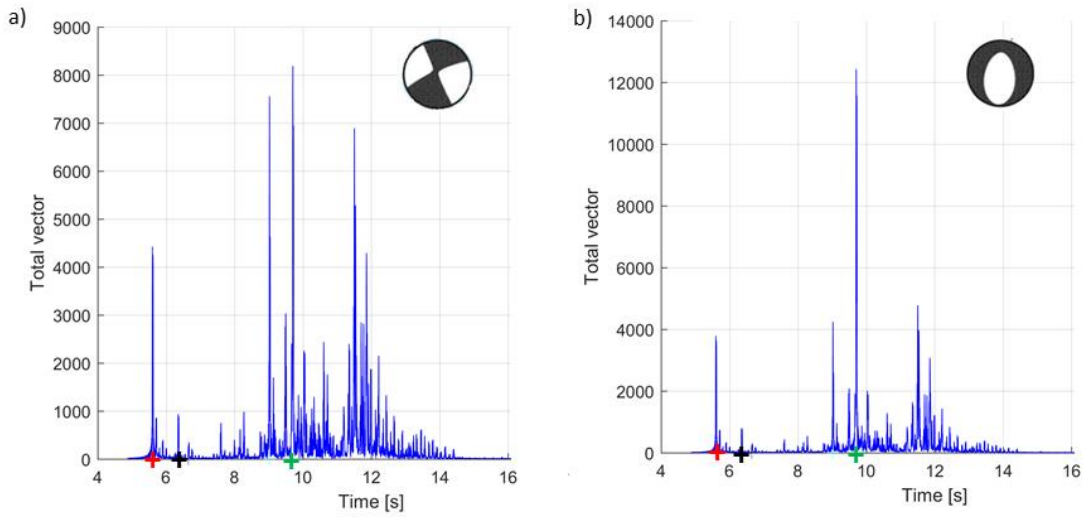

Figure S7. Synthetic total vectors for two different mechanisms. (a) Focal mechanism applied after *Stierle, Bohnhoff, and Vavryčuk* (2014) (their Table 3, mechanism 33); (b) focal mechanism applied after *Stierle, Bohnhoff, and Vavryčuk* (2014) (their Table 3, mechanism 16); both band-pass filtered by 1-10 Hz. The focal mechanisms are indicated. The depth of the event is at 11.5 km; its epicentral distance is 30 km. The horizontal interface has the positive velocity contrast with the velocity increase from 5 to 6 km s^{-1} at a depth of 4 km, and a velocity of 4 km s^{-1} down to a depth of 0.5 km simulating shallow weathered layer as reported for many areas (e.g., *Vavryčuk et al.*, 2004). The P-wave arrivals marked by the red crosses, the S-wave arrivals marked by the green crosses, the secondary phases marked by the black crosses. Note the differences in waveforms due to different focal mechanisms. Note the presence of many other phases due to the uppermost shallow layer of 0.5 km.

Cluster number	Weak/Strong	Flipped	Minor Phase	Major Phase	Correlation coef.	Number of events	Number of events in cluster to total number of events [%]	
			Time delay after P wave [s]	Time delay after P wave [s]				
2	Weak	Yes	0.50	0.85	0.46	11	0.85	
4,5,6,7	Weak	Yes	0.50	0.90	0.42	20	1.55	processed together
8	Weak	Yes	0.50	0.90	0.46	6	0.46	
9	Weak	Yes	0.70	0.90	0.37	13	1.01	
13	Weak	Yes	0.50	0.90	0.48	15	1.16	
17	Weak	Yes	0.50	1.00	0.46	79	6.15	
19	Weak	Yes	0.50	0.95	0.38	104	8.09	
20	Strong	Yes	0.50	0.95	0.79	15	1.16	
21	Strong	Yes	0.50	0.95	0.55	128	9.96	
22	Strong	Yes	0.50	0.90	0.80	18	1.4	
23	Strong	Yes	0.50	0.95	0.62	105	8.17	
24	Strong	Yes	0.50	0.90	0.64	23	1.79	
25	Strong	Yes	0.50	0.90	0.70	26	2.02	
26	Strong	Yes	0.50	0.90	0.61	14	1.09	
27	Strong	Yes	0.50	0.90	0.60	12	0.93	
28	Strong	Yes	0.50	0.95	0.56	42	3.27	
29	Strong	No	0.55	0.95	0.70	11	0.85	
30	Strong	Yes	0.55	0.95	0.70	44	3.42	
32	Strong	No	0.55	0.90	0.80	31	2.41	
33	Strong	No	0.50	0.90	0.73	105	8.17	
34	Strong	Yes	0.55	0.95	0.63	14	1.09	
36	Strong	No	0.55	0.90	0.82	65	5.06	
37	Strong	No	0.55	0.90	0.64	76	5.91	
38	Strong	No	0.55	0.90	0.60	6	0.46	
39	Strong	No	0.50	0.95	0.66	13	1.01	
40	Strong	No	0.55	0.90	0.63	29	2.25	
41	Strong	No	0.55	0.95	0.56	32	2.49	
42	Strong	No	0.60	0.90	0.54	186	14.48	
44	Strong	No	0.60	0.90	0.52	41	3.19	

Table S1. Details of the secondary phases for depth-sorted clusters at station GOK. The location of clusters is shown in Figure S1a; the original 45 spatially distributed clusters resulted in 32 clusters with a sufficient number of waveforms for data processing. Flipping of waveforms responds to consistency in the first-motion polarities in all vertical recordings and eliminates the effects of diversity of focal mechanisms. Arrival times of the phases were picked manually. Note the constant time delays of the secondary phases after the P wave independently of the cluster location. Weak/strong indicates the quality of the secondary phases in clusters after processing based on the correlation threshold of 0.5 and relates to Figure 7a. Correlation coefficients represent the mean value for all events in each cluster calculated in the time window of 0.7-1.1 s after the direct P wave (the time window of the major phase). The number of events in each cluster is indicated. The last column represents the percentage ratio between the number of events in each cluster to total number of events.

References

Allam, A. A., and Y. Ben-Zion (2012), Seismic velocity structures in the southern California plate-boundary environment from double-difference tomography, *Geophysical J. Int.*, 190(2), 1181-1196, doi: 10.1111/j.1365-246X.2012.05544.x

Jurkevics, A. (1988), Polarization analysis of three-component array data, *Bull. Seismol. Soc. Am.*, 78(5), 1725-1743

Stierle, E., M. Bohnhoff, and V. Vavryčuk (2014), Resolution of non-double-couple components in the seismic moment tensor using regional networks-II: application to aftershocks of the 1999 Mw 7.4 İzmit earthquake, *Geophys. J. Int.*, 196, 1878-1888, doi: 10.1093/gji/ggt503

Vavryčuk, V., P. Hrubcová, M. Brož, and J. Málek (2004), Azimuthal variation of Pg velocity in the Moldanubian, Czech Republic: Observations based on a multi-azimuthal common-shot experiment, *Tectonophysics*, 387, 189-203, doi: 10.1016/j.tecto.2004.06.015